IEEE Access
Multidisciplinary ⋮ Rapid Review ⋮ Open Access Journal

Received 29 March 2024, accepted 30 April 2024, date of publication 6 May 2024, date of current version 13 May 2024.

*Digital Object Identifier 10.1109/ACCESS.2024.3396909*

RESEARCH ARTICLE

# A New Reaching Law Based Nonsingular Terminal Sliding Mode Control Scheme for the Servo System With Periodic Uncertainties

**WEI CHEN[1], DEJIN TAO[2], AND BO TANG[1]**
[1]College of Electrical Engineering, Nanjing Vocational University of Industry Technology, Nanjing 210023, China
[2]The 28th Research Institute of China Electronics Technology Group Corporation, Nanjing 210000, China

Corresponding author: Wei Chen (supercw_86@163.com)

This work was supported in part by the Natural Science Foundation of Jiangsu Province under Grant BK20200493, and in part by the Start-Up Fund for New Talented Researchers of Nanjing Vocational University of Industry Technology under Grant YK23-02-04.

**ABSTRACT** A novel control strategy is introduced to optimize the position-tracking precision of the servo system in the face of disturbances and uncertainties, particularly periodic uncertainties that commonly exist in repetitively operating industrial equipment. Initially, in accordance with the tracking accuracy requirements, the position tracking error is divided into several error bands, and a new reaching law based on the error bands is established. The reaching law is composed of a linear term and a power term with variation coefficients. The proposed reaching law enhances the convergence rate of minor errors and mitigates inherent chattering. Subsequently, based on the new reaching law, a Non-Singular Terminal Sliding Mode Controller (NTSMC) with Periodic Adaptive Compensation (PAC) is developed. Amid periodic load torque variations and unmodeled system dynamics, the NTSMC component ensures rapid convergence of position tracking errors, while the PAC component improves tracking accuracy. The stability of the servo system under the proposed control law is analyzed using Lyapunov theory. Both simulations and experimental results demonstrate that high-precision tracking performance can be realized under various load situations.

**INDEX TERMS** Error bands based reaching law, periodic uncertainties, periodic adaptive control, non-singular terminal sliding mode control.

## I. INTRODUCTION

Servo systems equipped with Permanent Magnet Synchronous Motors (PMSMs) have gained significant attention in various industrial applications due to their high efficiency, high accuracy, and excellent dynamic performance [1], [2], [3]. In practical applications, servo systems are often affected by parameter perturbations and load torque uncertainties [4], [5]. The load torque uncertainties, categorized into periodic and non-periodic uncertainties, can severely degrade the tracking performance of the systems. In particular, periodic uncertainties, such as torque ripples and speed fluctuations in servo systems, can affect tracking performance and cause undesired vibrations and noise. However, periodic uncertainties are very common in servo systems such as mechanical arms and surface mounting equipment that work in a repetitive or periodic manner. In such situations, traditional linear controllers, such as the PI controller, cannot achieve satisfactory results, especially when high tracking accuracy is required.

To enhance the control accuracy and robustness of the servo systems, various modern control techniques, such as neural network control [6], sliding mode control [7], fuzzy control [8], adaptive control [9], adaptive robust control [10], reinforcement learning control [11], active disturbance rejection control [12] and observer-based methods [13], [14] were developed and implemented. The methods mentioned above can improve the servo system performance in different ways.

The associate editor coordinating the review of this manuscript and approving it for publication was Xiwang Dong.

Of all the methods mentioned above, the sliding mode control (SMC) method has gained widespread concern in the servo control field due to its implementation ability and robustness against uncertainties and disturbances. These features make SMC particularly suitable for high-performance applications where precise control of motor position and speed is required. In [15], a sliding-mode based nonlinear control scheme for PMSM servo systems was developed. The proposed disturbance observer, which is based on sliding mode techniques, can compensate for strong disturbances and achieve high servo precisions. In [16], a fuzzy sliding mode speed controller was developed, a load torque observer was also designed, the speed control performance of a PMSM under parameter perturbations and load torque variations was greatly improved. In recent years, the dynamic performance of SMC techniques applied in servo systems has been improved in two ways. One is introducing nonlinear sliding surfaces to guarantee finite-time convergence of the tracking errors, such as terminal sliding mode control (TSMC) [17]. The other is reducing the chattering phenomenon by improving the convergence rate [18] or introducing higher-order sliding mode control techniques [19]. When the disturbance varies in a small range, simply using SMC can mitigate its impact. However, when the disturbance spans a wide range, utilizing SMC alone is not enough. This is because if only the SMC method is used, a significant increase in the switching gain is required. It can cause serious chattering. Furthermore, large switching gains are difficult to implement in real systems, so promising tracking performance cannot be achieved. In this situation, additional compensation is needed. In addition, when the tracking error is small, especially in the neighborhood of the balance point, the convergence rate is slowed down. It also needs to be improved.

Some recent results on disturbance rejection have been developed in literature [20], [21], [22], [23], [24], [25], [26]. A robust consensus control method for multi-agent with unknown control directions was developed in [20] and [21]. The method can also be applied to uncertain robotic manipulators. Velocity and torque constraints were taken into consideration and the asymptotic stability of the closed loop system can be guaranteed. Fuzzy adaptive and finite-time adaptive fault-tolerant control methods were developed in [22] and [23]. The methods can handle a class of novel actuator faults - input power faults well. System states under fault conditions can converge to a small neighborhood of the origin under the effort of these methods. In [24] and [25], periodic piecewise systems with input delays and external disturbances were studied. Actuator saturations, immeasurable states and other uncertainties were also taken into consideration, anti-windup compensator-based and proportional integral observer-based controllers were developed respectively, which can guarantee the stability of the systems. In [26], the synchronization problem of multiple memristor-based neural networks with disturbances, parameter uncertainties and actuator faults was studied, and an observer-based estimator and the H-infinity control method were incorporated in the unified controller to deal with matched and mismatched disturbances respectively. However, these methods are not specifically designed for periodic unmodeled dynamics, thus, they are less suitable for the operating situations that the load torque spans a wide range.

Motivated by the analysis above, and to mitigate the impact of parameter uncertainties and load torque variations, especially periodic uncertain load torque that spans a wide range, a non-singular terminal sliding mode-based position tracking control scheme with periodic adaptive compensation is proposed. First, a new reaching law based on the error bands is developed. The reaching law is composed of a linear term and a power term with variation coefficients. The designed reaching law can improve the convergence rate of small errors and suppress the inherent chattering. Then, based on the new reaching law, a non-singular terminal sliding mode periodic adaptive control scheme is developed. The periodic characteristic of the disturbance is utilized to design a compensator to improve the tracking accuracy of the servo systems under large-scale periodic disturbances. The control scheme also consists of two parts, i.e., the NTSMC term and the periodic adaptive compensation (PAC) term. The fast convergence of tracking error and robustness of the servo system against parameter variations is guaranteed by the NTSMC term. The tracking accuracy is further enhanced by the periodic adaptive compensation term, which approximates the periodic dynamics of the system with high precision. The effectiveness of the proposed control scheme is validated by simulation and experimental results. In summary, the main contributions of this work are summarized as follows:

1) An error bands based new reaching law for NTSMC is developed in this paper. The NTSMC is used to mitigate the impact of small parameter variations. However, when the periodic uncertainties that commonly exist in industrial applications span a wide range, the NTSMC cannot handle them well. To address the problems above, a robust control scheme that composed of an NTSMC component and a periodic adaptive compensation (PAC) component is proposed for the servo systems with periodic uncertainties. Besides, to improve the error convergence rate in the neighborhoods of the balance point, a new error bands based reaching law is proposed. The method is simple in structure and is easy to implement in practical applications.

2) An adaptive compensator that can approximate the periodic uncertainties is developed. It can significantly enhance the tracking accuracy of the servo systems under periodic uncertainties. As a result of the compensator, a large switch gain of the SMC is not needed, so the chattering phenomenon is reduced. This is very useful in real applications.

3) In addition, the stability of the servo system under the control law is proved. The effectiveness of the proposed control method is verified by comparative simulations and experiments. The control scheme can achieve high tracking accuracy under different load conditions.

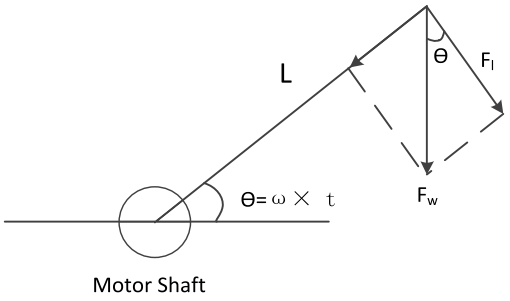


**FIGURE 1.** Torque analysis of the motor shaft.

The remainder of this article is organized as follows. In Section II, the mathematical model of the servo system is formulated. In section III, the proposed controller is designed and the system stability is analyzed. Section IV and Section V show the simulation and experimental results respectively. Finally, some conclusions are given in Section VI.

## II. MATHEMATICAL MODEL OF THE SERVO SYSTEM

In many servo applications, the load torque acting on the system is always in one direction. When the servo system uses a direct drive permanent magnet synchronous motor (DDPMSM), the analysis of the torque applied to the motor rotor is shown in Figure 1, where $\theta$ is the angle of the motor rotor, $\omega$ is the speed of the motor, $t$ is the running time, $F_w$ is the force acting on the servo system, $F_l$ is the component of $F_w$, which is perpendicular to the force arm, $L$ is the length of the force arm. From Figure1, the uncertain torque $f_{rp}(t)$ of the DDPMSM can be derived as follows:

$$f_{rp}(t) = F_l(t)L = F_w\cos(\theta)L = F_wL\cos(\omega t) \quad (1)$$

From equation 1 it can be found that $f_{rp}(t)$ is a periodic torque, the period is related to the motion speed. Typically, the armature equations of DDPMSM in the rotating coordinate system can be expressed as follows [27]:

$$U_d = L\frac{di_d}{dt} + Ri_d - n_p\omega Li_q \quad (2)$$

$$U_q = L\frac{di_q}{dt} + Ri_q + \omega_e Li_d + n_p\omega\varphi_m \quad (3)$$

where $U_d$, $U_q$ are stator voltages of the d-axis and the q-axis; $i_d$, $i_q$ are stator currents of the two axes, $R$ is the stator resistance, $L$ is the stator inductance, and $\varphi_m$ is the rotor flux linkage; $n_p$ is the pole pairs of the motor; $\omega$ is the angular velocity of the motor rotor.

The torque equation of the motor is:

$$T_e = \frac{3}{2}n_p\varphi_m i_q \quad (4)$$

where $T_e$ is the electromagnetic torque. Then motion equation of the DDPMSM can be derived as:

$$J\frac{d\omega}{dt} = T_e - T_L - f_{rp}(t) - f_\Delta(t) \quad (5)$$

where $J$ is the moment of inertia, $T_L$ is a constant load torque, $f_{rp}(t)$ is the periodic uncertain dynamics which represent unknown periodic load torque, speed fluctuations, harmonics, etc.. $f_\Delta(t)$ represents the non-periodic unmodeled dynamics. When the feed-forward decoupling control algorithm [28] and back EMF compensation [29] are implemented in the current loop, then equation (2) and (3) can be simplified as:

$$U_d = L\frac{di_d}{dt} + Ri_d \quad (6)$$

$$U_q = L\frac{di_q}{dt} + Ri_q \quad (7)$$

In the Field-Orient Control (FOC) strategy, $i_d = 0$ control scheme is often used. In this case, only equation (7) needs to be considered. When the PI controller is used and the control parameters are well-tuned in the current loop, the pole of the model can be canceled by the zero of the PI controller. Therefore, the current $i_q$ is nearly proportional to the control voltage $U_q$. Let the scale factor be $k_c$, then the model of the servo system can be derived as:

$$\begin{cases} \dfrac{d\theta(t)}{dt} = \omega(t) \\ \dfrac{d\omega(t)}{dt} = \dfrac{K_t}{J}u_q(t) - \dfrac{T_L}{J} - f_{rp}(t) - f_\Delta(t) \end{cases} \quad (8)$$

where $K_t$ is the torque constant of the motor:

$$K_t = \frac{3}{2}n_p\varphi_m k_c \quad (9)$$

Since $f_{rp}(t)$ is the periodic unknown dynamics, it meets the following condition:

$$f_{rp}(t) = f_{rp}(t-T)\, t > T\,(T = \frac{2\pi}{\omega(t)}) \quad (10)$$

where T is the period of the unknown dynamics. It depends on the rotating speed of the motor. It is calculated at the beginning of each period. The following assumptions are made for the desired position trajectories $\theta_d(t)$, the periodic unknown dynamics $f_{rp}(t)$ and the unmodeled dynamics $f_\Delta(t)$:

*Assumption 1:* The second-order derivation of the desired position trajectories $\theta_d(t)$ exists.

*Assumption 2:* The periodic unknown dynamics $f_{rp}(t)$ is bounded; The unmodeled dynamics $f_\Delta(t)$ is also bounded, assuming its upper limit is $\rho$, that is $|f_\Delta(t)| < \rho$.

*Remark 1:* In most industrial applications, the servo system is used to track a predetermined position trajectory. In order to ensure the smoothness of the operation, both the velocity and acceleration cannot change abruptly. As the first order derivative of position is velocity and the second order derivative is acceleration, in practical applications, assumption 1 can be met. Besides, during the operation process, the load torque imposed on the motor is bounded, the motor parameters always vary within a certain range, so assumption 2 can also be met.

This paper aims to design the control law $u_q(t)$ to overcome the effect of $f_{rp}(t)$ and $f_\Delta(t)$. The control objective is that the rotor position $\theta(t)$ can track the desired position trajectories $\theta_d(t)$ despite the existing periodic unknown dynamics $f_{rp}(t)$ and unmodeled dynamics $f_\Delta(t)$, the tracking error converges.

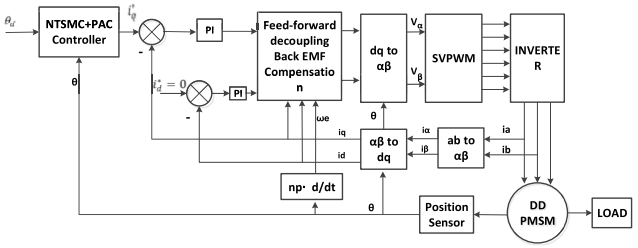


**FIGURE 2.** The control scheme of the proposed method.

## III. CONTROLLER DESIGN AND STABILITY ANALYSIS

A novel position controller is developed to improve the performance of the servo system influenced by the periodic uncertainties and unmodeled dynamics in this paper. A traditional PI controller with feed-forward decoupling items and back EMF compensation is used in the current loop. This section mainly focuses on the design of the non-singular terminal sliding mode-based position controller with periodic adaptive compensation. The structure of the proposed control scheme is shown in Fig.2

### A. ERROR BANDS BASED REACHING LAW

To speed up the convergence rate of the small errors and reduce the chattering phenomenon, an error bands based reaching law is proposed as:

$$\dot{s}(t) = -k_1 s(t) - \max(k_2, k_2 \left|\frac{\varepsilon}{s(t)}\right|^{\alpha}) \text{sign}[s(t)] \left|\frac{s(t)}{\varepsilon}\right|^{\alpha^{sign\left(\left|\frac{s(t)}{\varepsilon}\right|-1\right)}} \tag{11}$$

where $s(t)$ denotes the sliding mode surface, $k_1, k_2$ is the gain of the sliding mode control law, $k_1 > 0$, $k_2 > 0$, $\varepsilon$ denotes the boundary of the large and small error bands $\varepsilon > 0$. $\alpha$ is the power index and $\alpha > 1$. The analysis of the reaching law is as follows:

(1) When $\left|\frac{s(t)}{\varepsilon}\right| > 1$, that is $s(t)$ is within the large error band, in this situation $\text{sign}\left(\left|\frac{s(t)}{\varepsilon}\right| - 1\right) = 1$ and $\left|\frac{\varepsilon}{s(t)}\right| < 1$, as $\alpha > 1$ and $k_2 > 0$, thus $\max\left(k_2, k_2 \left|\frac{\varepsilon}{s(t)}\right|^{\alpha}\right) = k_2$, according to (11) the reaching law is:

$$\dot{s}(t) = -k_1 s(t) - k_2 \text{sign}[s(t)] \left|\frac{s(t)}{\varepsilon}\right|^{\alpha} \tag{12}$$

Obviously, (12) is a fast power reaching law. The convergence rate is magnified by the power $\alpha$.

(2) When $0 < \left|\frac{s(t)}{\varepsilon}\right| \leq 1$, that is $s(t)$ is within the small error band, in this situation $\text{sign}\left(\left|\frac{s(t)}{\varepsilon}\right| - 1\right) = -1$ and $\left|\frac{\varepsilon}{s(t)}\right| > 1$, as $\alpha > 1$ and $k_2 > 0$, thus $\max\left(k_2, k_2 \left|\frac{\varepsilon}{s(t)}\right|^{\alpha}\right) = k_2 \left|\frac{\varepsilon}{s(t)}\right|^{\alpha}$,then the reaching law is changed to:

$$\begin{aligned}\dot{s}(t) &= -k_1 s(t) - k_2 \left|\frac{\varepsilon}{s(t)}\right|^{\alpha} \text{sign}[s(t)] \left|\frac{s(t)}{\varepsilon}\right|^{\frac{1}{\alpha}} \\ &= -k_1 s(t) - k_2 \text{sign}[s(t)] \left|\frac{\varepsilon}{s(t)}\right|^{\alpha - \frac{1}{\alpha}}\end{aligned} \tag{13}$$

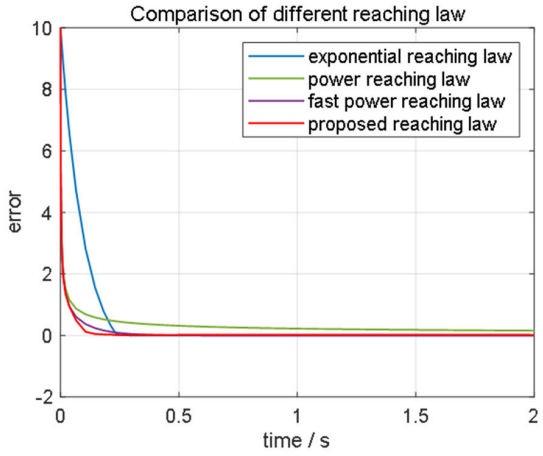


**FIGURE 3.** Comparison of different reaching law.

In this situation, it can be found that although $s(t)$ is in the small error band, the convergence rate is enlarged by the term $\left|\frac{\varepsilon}{s(t)}\right|^{\alpha - \frac{1}{\alpha}}$. The convergence speed remains high despite $s(t)$ decreases greatly. The convergence speed of different reaching laws are compared in Fig. 3, the proposed reaching law provides the fastest convergence speed when the error is small.

### B. DESIGN OF THE CONTROLLER

The position tracking error of the servo system is defined as:

$$e(t) = \theta_d(t) - \theta(t) \tag{14}$$

Then, the non-singular terminal sliding mode surface is designed as:

$$s(t) = e(t) + r\dot{e}(t)^{p/q} \tag{15}$$

where $r > 0$, $p$ and $q$ are positive odd integers, and $1 < \frac{p}{q} < 2$. Usually, we choose adjacent odd numbers as the values of $p$ and $q$, for example $p = 5$, $q$=3 or $p = 11$, $q$=9, etc. It should be noted that that as the value of $\frac{p}{q}$ decreases, the error converges faster, but it is also more likely to cause oscillations in the error. It is proved by [30] that the sliding mode surface converges in finite time. For system (8), the control law $u_s(t)$ is designed as:

$$u_s(t) = u_m(t) + u_{rb}(t) \tag{16}$$

$u_m(t)$ is the control law for the nominal model, which is designed as:

$$u_m(t) = \frac{J}{K_t}\left[\frac{q}{rp}\dot{e}^{\left(2-\frac{p}{q}\right)}(t) + \ddot{\theta}_d(t) + \frac{T_L}{J}\right] \tag{17}$$

The sliding mode control law $u_{rb}(t)$ is designed as:

$$u_{rb}(t) = \frac{J}{K_t}\left\{k_1 s(t) + \max\left(k_2, k_2 \left|\frac{\varepsilon}{s(t)}\right|^{\alpha}\right) \text{sign}[s(t)] \left|\frac{s(t)}{\varepsilon}\right|^{\alpha^{sign\left(\left|\frac{s(t)}{\varepsilon}\right|-1\right)}}\right\} \tag{18}$$

where $k_1 > 0$, $k_2 \geq \rho$, $\alpha > 1$. $\varepsilon > 0$. sign$(\cdot)$ denotes the sign function, since this function is not a continuous one, it can cause a chattering phenomenon. In practical applications, the continuous sigmod function is usually used to suppress the chattering phenomenon by replacing the sign function, which is defined as:

$$\text{sigmod}(s) = \frac{2}{1+e^{-s}} - 1 \tag{19}$$

The periodic adaptive compensation term $u_{rp}(t)$, which can compensate for the effect of the periodic load torque, is designed as:

$$u_{rp}(t) = \frac{J}{2K_t}[\hat{f}_{rp}(t) + \hat{f}_{rp}(t-T)] \tag{20}$$

In equation (20), $\hat{f}_{rp}(t)$ and $\hat{f}_{rp}(t-T)$ denote the estimation of $f_{rp}(t)$ in this and previous cycle respectively. The adaptive rate of $\hat{f}_{rp}(t)$ is designed as:

$$\hat{f}_{rp}(t) = \begin{cases} \hat{f}_{rp}(t-T) + r_{adp}\dfrac{rp}{2q}\dot{e}^{\left(\frac{p}{q}-1\right)}(t)\, s(t) & t > T \\ 0 & t < T \end{cases} \tag{21}$$

where $r_{adp}$ is the gain of the periodic adaptive compensation. Thus, the control law $u_q(t)$ can be derived as:

$$u_q(t) = u_s(t) + u_{rp}(t) = u_m(t) + u_{rb}(t) + u_{rp}(t) \tag{22}$$

### C. STABILITY ANALYSIS

*Theorem 1:* Assume the system (8) satisfies Assumption 1 and 2. When the servo system is tracking the desired trajectory $\theta_d(t)$ under the effect of the control law (22), the position error of the system converges to zero.

*Proof:* When $t > T$, consider the Lyapunov function:

$$V(t) = V_1(t) + V_2(t) \tag{23}$$

$$V_1(t) = \frac{1}{2}s^2(t) \tag{24}$$

$$V_2(t) = \frac{1}{r_{adp}}\int_{t-T}^{t}[f_{rp}(\tau) - \hat{f}_{rp}(\tau)]^2 d\tau \tag{25}$$

According to equation (14), $\ddot{e}(t)$ can be derived as:

$$\ddot{e}(t) = \ddot{\theta}_d(t) - \ddot{\theta}(t) = \ddot{\theta}_d(t) - \dot{\omega}(t) \tag{26}$$

By substituting system model (8) into equation (26) yields:

$$\ddot{e}(t) = \ddot{\theta}_d(t) - \frac{K_t}{J}u_q(t) + \frac{T_L}{J} + f_{rp}(t) + f_\Delta(t) \tag{27}$$

By substituting equation (16) (17) (18) (20), then equation (27) can be rewritten as:

$$\begin{aligned}\ddot{e}(t) = &-k_1 s(t) - \frac{q}{rp}\dot{e}^{\left(2-\frac{p}{q}\right)}(t) \\ &+ f_{rp}(t) - \frac{1}{2}\left[\hat{f}_{rp}(t) + \hat{f}_{rp}(t-T)\right] + f_\Delta(t) \\ &- \max\left(k_2, k_2\left|\frac{\varepsilon}{s(t)}\right|^\alpha\right)\text{sign}[s(t)]\left|\frac{s(t)}{\varepsilon}\right|^{\alpha^{sign\left(\left|\frac{s(t)}{\varepsilon}\right|-1\right)}}\end{aligned} \tag{28}$$

Taking the derivative of the sliding mode surface (15), yields:

$$\begin{aligned}\dot{S}(t) &= \dot{e}(t) + \frac{rp}{q}\dot{e}^{\left(\frac{p}{q}-1\right)}(t)\,\ddot{e} \\ &= \frac{rp}{q}\dot{e}^{\left(\frac{p}{q}-1\right)}(t)\left[\frac{q}{rp}\dot{e}^{\left(2-\frac{p}{q}\right)}(t) + \ddot{e}(t)\right]\end{aligned} \tag{29}$$

Combining equation (28) and (29) we have:

$$\begin{aligned}\dot{s}(t) = &\frac{rp}{q}\dot{e}^{\left(\frac{p}{q}-1\right)}(t) - k_1 s(t) \\ &+ f_{rp}(t) - \frac{1}{2}\left[\hat{f}_{rp}(t) + \hat{f}_{rp}(t-T)\right] + f_\Delta(t) \\ &- \max(k_2, k_2\left|\frac{\varepsilon}{s(t)}\right|^\alpha)\text{sign}[s(t)]\left|\frac{s(t)}{\varepsilon}\right|^{\alpha^{sign\left(\left|\frac{s(t)}{\varepsilon}\right|-1\right)}}\}\end{aligned} \tag{30}$$

Taking the derivative of the function (24) and considering (29) yields:

$$\begin{aligned}\dot{V}_1(t) = s(t)\,\dot{s}(t) = &\frac{rp}{q}\dot{e}^{\left(\frac{p}{q}-1\right)}(t)\{-k_1 s^2(t) \\ &+ \frac{1}{2}s(t)[2f_{rp}(t) - \hat{f}_{rp}(t) - \hat{f}_{rp}(t-T)] + s(t)f_\Delta(t) \\ &- \max(k_2, k_2\left|\frac{\varepsilon}{s(t)}\right|^\alpha)\text{sign}[s(t)]\left|\frac{s(t)}{\varepsilon}\right|^{\alpha^{sign\left(\left|\frac{s(t)}{\varepsilon}\right|-1\right)}}\end{aligned} \tag{31}$$

Taking derivative of the function (25) yields:

$$\begin{aligned}\dot{V}_2(t) = \frac{1}{r_{adp}}&\left\{\left[f_{rp}(t) - \hat{f}_{rp}(t)\right]^2\right. \\ &\left. - \left[f_{rp}(t-T) - \hat{f}_{rp}(t-T)\right]^2\right\}\end{aligned} \tag{32}$$

By using (10), equation (32) can be given as:

$$\begin{aligned}\dot{V}_2(t) = -\frac{1}{r_{adp}}&[\hat{f}_{rp}(t) - \hat{f}_{rp}(t-T)]\{2f_{rp}(t) \\ &-[\hat{f}_{rp}(t) + \hat{f}_{rp}(t-T)]\}\end{aligned} \tag{33}$$

Substituting the adaptive rate (21) into (33) yields:

$$\dot{V}_2(t) = -\frac{rp}{2q}\dot{e}^{\left(\frac{p}{q}-1\right)}(t)\, s(t)\{2f_{rp}(t) - [\hat{f}_{rp}(t) + \hat{f}_{rp}(t-T)]\} \tag{34}$$

Considering (31) and (34), the first order time derivative of Lyapunov function (23) can be given as:

$$\begin{aligned}\dot{V}(t) &= \dot{V}_1(t) + \dot{V}_2(t) \\ &= \frac{rp}{q}\dot{e}^{\left(\frac{p}{q}-1\right)}(t)\left[-k_1 s^2(t) + s(t)f_\Delta(t)\right. \\ &\quad \left. - \max(k_2, k_2\left|\frac{\varepsilon}{s(t)}\right|^\alpha)\text{sign}[s(t)]\left|\frac{s(t)}{\varepsilon}\right|^{\alpha^{sign\left(\left|\frac{s(t)}{\varepsilon}\right|-1\right)}}\right]\end{aligned} \tag{35}$$

Since $p$ and $q$ are positive odd integers and satisfy the condition $1 < \frac{p}{q} < 2$, it can be obtained that $\frac{p}{q}\dot{e}^{\left(\frac{p}{q}-1\right)} > 0$. Considering $|f_\Delta(t)| < \rho$ and $k_2 \geq \rho$, $\alpha > 1$, when $|s(t)|$ is in the range of the large error band, that is $|s(t)| > \varepsilon$, it can be derived that:

$$\begin{aligned}\dot{V}(t) &\leq \frac{rp}{q}\dot{e}^{\left(\frac{p}{q}-1\right)}(t)\left\{-k_1 s^2(t)+\rho|s(t)|\left[1-\left|\frac{s(t)}{\varepsilon}\right|^{\alpha}\right]\right\} \\ &\leq -k_1\frac{rp}{q}\dot{e}^{\left(\frac{p}{q}-1\right)}(t)\,s^2(t) \end{aligned} \tag{36}$$

When $|s(t)|$ is in the range of the small error band, that is $|s(t)| \leq \varepsilon$, then:

$$\begin{aligned}\dot{V}(t) &\leq \frac{rp}{q}\dot{e}^{\left(\frac{p}{q}-1\right)}(t)\left\{-k_1 s^2(t)\right. \\ &\quad \left.+\rho|s(t)|\left[1-\left|\frac{\varepsilon}{s(t)}\right|^{\alpha-\frac{1}{\alpha}}\right]\right\} \\ &\leq -k_1\frac{rp}{q}\dot{e}^{\left(\frac{p}{q}-1\right)}(t)\,s^2(t) \end{aligned} \tag{37}$$

Further considering $k_1 > 0$ and $r > 0$, the following inequality holds:

$$\dot{V}(t) < 0 \tag{38}$$

Integrating both sides of inequality (36), (37) yields:

$$V(t) = V(T) - \int_T^t k\frac{rp}{q}\dot{e}^{\left(\frac{p}{q}-1\right)}(\tau)\,s^2(\tau)\,d\tau < V(T) \tag{39}$$

Then, $V(T)$ can be obtained from (23) $\sim$ (25) that:

$$\begin{aligned}V(T) &= V_1(T) + V_2(T) \\ &= \frac{1}{2}s^2(T) + \int_0^T f_{rp}^2(\tau)\,d\tau < +\infty \end{aligned} \tag{40}$$

It is indicated by (38) $\sim$ (40) that $V(t)$ together with $V_1(t)$ and $V_2(t)$ is bounded by $V(T)$ and will converge to zero exponentially. Therefore, based on the discussions above, we can conclude that the position tracking error $e(t)$ converges.

## IV. SIMULATION RESULTS

Simulations are performed in MATLAB to investigate the performance of the proposed controller. In the simulations, four controllers are used for position tracking performance comparison, including the traditional PI controller, the PI controller combined with periodic adaptive compensation (PI+PAC), the non-singular terminal sliding mode controller (NTSMC), and the non-singular terminal sliding mode controller combined with periodic adaptive compensation (NTSMC+PAC). In the current loop, the traditional PI controller is used. The gain of the proportional and integral terms is set as $k_{pc}$= 17, $k_{ic}$= 5600 respectively. The parameters of the current loop controller remain consistent when the position/velocity controller changes. The servo system is tested for tracking a 62.8 rad/s position command, which is shown in Figure 4. The load is directly driven by the servo motor. The constant load torque is set to $T_L$= 2N · m, the unknown periodic load torque varies in different simulation cases to verify controller performance. The parameters of the controllers are well-tuned to achieve similar performance under simulation case I. All parameters used in the simulation are listed in Table 1. The parameters of the controllers remain consistent in different simulation cases and the results are shown in Figure 5- Figure 7.

In simulation case I, the unknown periodic load torque is set as $f_{rp}(t) = 2\sin(\theta)$N · m, whose maximum value is equal to the constant load torque. Position tracking errors are shown in Figure 5a. The performances of the four controllers are similar: the maximum error is about 0.03 rad, and the steady errors are almost the same. However, small differences can be found in the enlarged pictures. Due to the nonlinear factor,

**TABLE 1. Parameters of the simulation.**

| | |
|---|---|
| Model Parameters | |
| DC bus voltage $V_{dc}$ | 311 V |
| PWM frequency | 10 kHz |
| Motor type | PMSM |
| Motor stator resister $R$ | 2.8 Ω |
| Motor inductance $L_d$ $L_q$ | 8.5 mH |
| Motor Flux Linkage $\varphi$ | 0.175 Vs |
| Motor Torque Constant $K_t$ | 1.05 N · m/A |
| Motor inertia $J$ | $3 \times 10^{-3}$ kg · m$^3$ |
| Viscous damping $F_v$ | 0.008 N · m · s |
| number of pole pairs | 4 |
| Load Conditions | |
| Constant load torque $T_L$ | 2 N · m |
| Case I: $f_{rp}(t)$ | 2sin(·) N · m |
| Case II: $f_{rp}(t)$ | 4sin(·) N · m |
| Case III: $f_{rp}(t)$ | 6sin(·) N · m |
| Current PI Controller Parameters | |
| Current loop $k_{pc}$ | 17 |
| Current loop $k_{ic}$ | 5600 |
| Position/ Velocity PI Controller Parameters | |
| Velocity loop $k_{pv}$ | 6.0 |
| Velocity loop $k_{iv}$ | 0.05 |
| Position loop $k_{pp}$ | 200 |
| Position loop $k_{ip}$ | 2000 |
| NTSMC+PAC controller | |
| $r$ | 0.01 |
| $\varepsilon$ | 0.1 |
| $p$ | 21 |
| $q$ | 19 |
| $k_1$ | 8000 |
| $k_2$ | 1200 |
| $r_{adp}$ | 4000 |

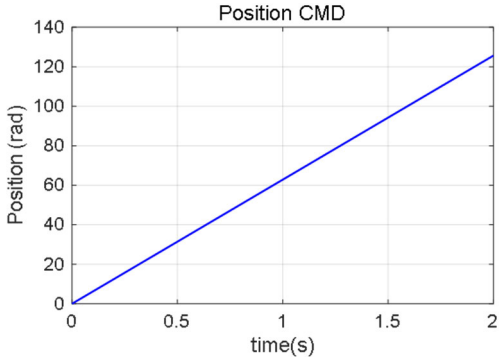


**FIGURE 4.** Position command.

the error convergence speed of NTSMC is much faster than that of the PI controller. The periodic adaptive compensation term is shown in Figure 5b, which can gradually compensate for the periodic load torque disturbance. Owing to its effect, the minimum position tracking error in the steady state is obtained by the proposed method. The speed and torque response of the motor under the effect of the NTSMC+PAC are shown in Figure 5c and Figure 5d respectively.

In simulation case II, the unknown periodic load torque is increased to $f_{rp}(t) = 4\sin(\theta)$ N·m, tracking errors of the four controllers are compared in Figure 6a. As the periodic load doubles, the maximum errors of the four controllers remain the same. However, in the steady state, the tracking errors of the PI controller and the NTSMC increase. As the periodic load exceeds the boundary of the preset gain, there is a significant deterioration in the control performance of NTSMC. By adding the periodic adaptive compensation part shown in Figure 6b, the steady performance of the controllers improves greatly. Owning to the sliding mode control technology, the control performance of NTSMC+PAC is better than that of PI+PAC.

In simulation case III, the unknown periodic load torque continues to increase to $f_{rp}(t) = 6\sin(\theta)$ N·m, which is three times the simulation case I. The position tracking errors of the PI controller and the NTSMC continue to increase. There is a large error increase of NTSMC when the load disturbance exceeds the boundary of the preset gain, The proposed method can overcome the defects of the NTSMC by introducing the PAC term. The simulation results indicate that the proposed NTSMC+PAC controller has the best disturbance rejection ability to unknown periodic dynamics of all the four controllers.

## V. EXPERIMENTAL RESULTS

To further verify the effectiveness of the proposed control strategy, experiments are also carried out under the platform shown in Figure 8. The experimental system is composed of a computer, a DSP controller and drive pack, a low-voltage servo motor, and a DC voltage regulator. The DSP development board LAUNCHXL-F28069, a production of Texas Instruments (TI) company, is used as the real-time controller.

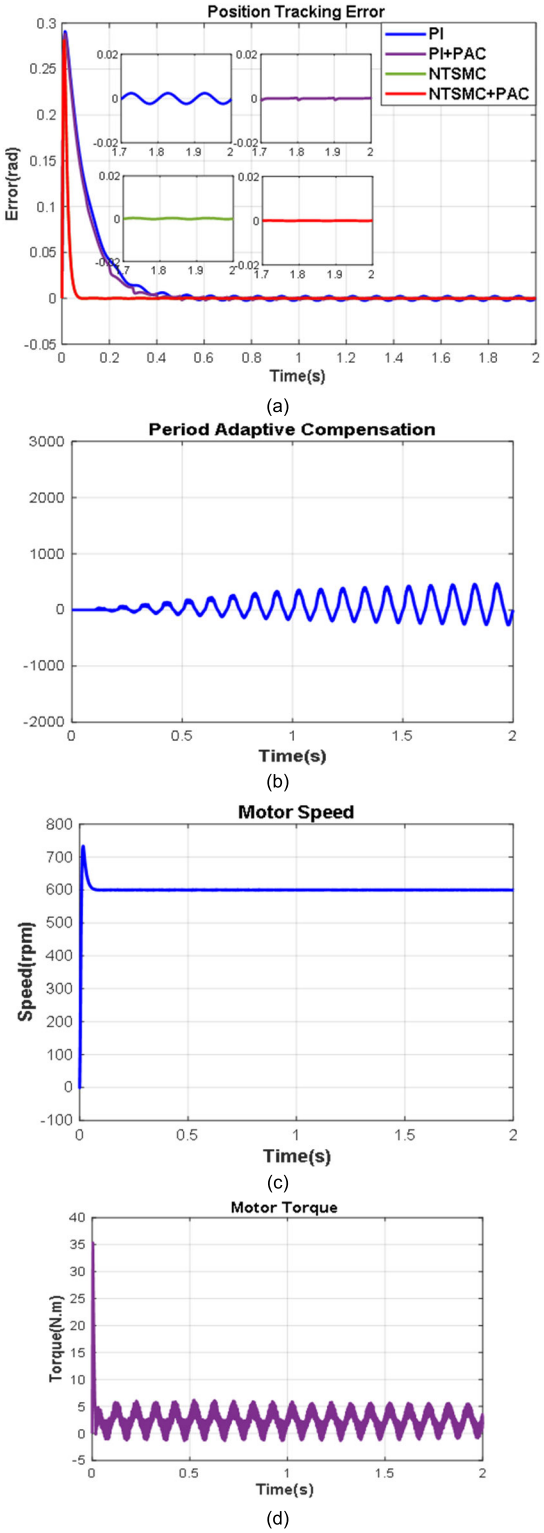


**FIGURE 5.** Simulation case I: $f_{rp}(t) = 2sin(\theta)$ N·m. (a) Position Error of different controllers. (b) PAC term. (c) Motor speed. (d) Motor torque.

All the control algorithms are written in the Code Composer Studio 6 environment. The code is compiled, generated by the computer, and then downloaded to the development board.

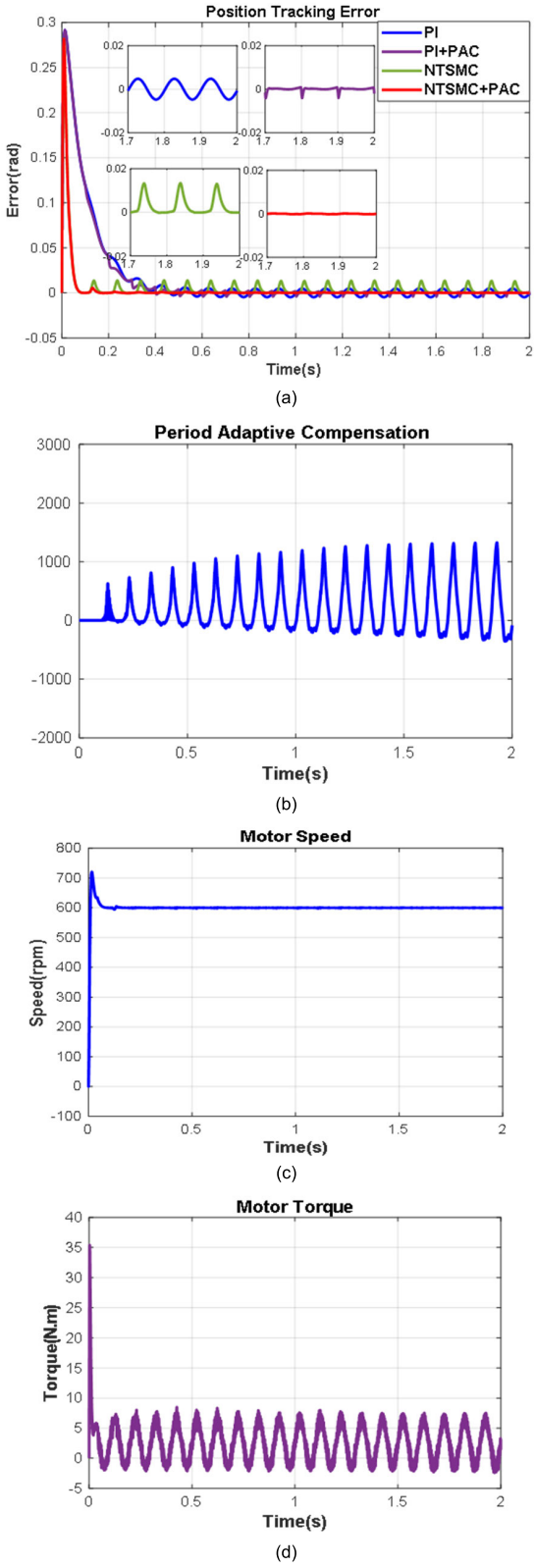


**FIGURE 6.** Simulation case II: $f_{rp}(t) = 4sin(\theta)$ N·m. (a) Position Error of different controllers. (b) PAC term. (c) Motor Speed. (d) Motor torque.

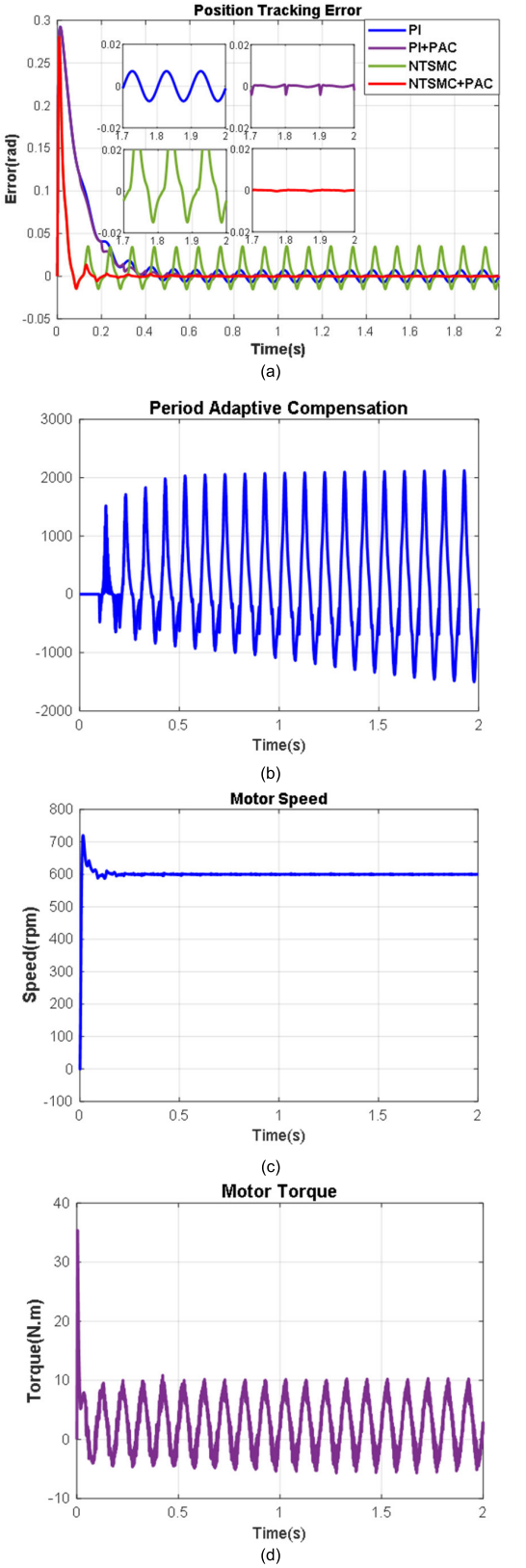


**FIGURE 7.** Simulation case III: $f_{rp}(t) = 6sin(\theta)$ N·m. (a) Position Error of different controllers. (b) PAC term. (c) Motor Speed. (d) Motor torque.

The drive pack, whose model is BOOSTXL-DRV8305EVM is a 3-phase driver stage. The pack supports a 4.4 V to 45 V voltage supply and up to 15 A drive current. It is usually docked with LAUNCHXL for motor application evaluations.


(a) (b) (c)

**FIGURE 8.** Experimental platform. (a) platform. (b) periodic load1. (c) periodic load2.

**TABLE 2.** Parameters of the PMSM.

| Motor Parameters | Units | Value |
|---|---|---|
| Rated Voltage | V | 36 |
| Rated Power | W | 200 |
| Rated Torque | N · m | 0.64 |
| Rated Speed | rpm | 3000 |
| Rated Current | A | 7.1 |
| Pole pairs | | 5 |
| Rotor Inertia | kg · m$^2$ | 0.32× $10^{-3}$ |
| Torque Coefficient | N · m/A | 0.09 |
| Line Resistant | Ω | 0.4 |
| Line Inductance | mH | 0.7 |
| Encode Resolution | PPR | 1250 |

**TABLE 3.** Periodic load conditions.

| Load Parameters | Units | Value |
|---|---|---|
| Load1 Inertia | kg · m$^2$ | 1.65× $10^{-3}$ |
| Load1 Max Torque | N · m | 0.05 |
| Load2 Inertia | kg · m$^2$ | 3.56× $10^{-3}$ |
| Load2 Max Torque | N · m | 0.16 |

In the experiments, a 30 V/5 A DC voltage regulator is used as the power. A low-voltage servo motor, whose parameters are listed in Table 2, is used to drive the load directly. An iron bar mounted directly on the motor shaft can provide periodic load torque when the motor spins. As shown in Figure 8, load torque and inertia can be adjusted by using different fixing holes.

The experiments are conducted under two load conditions. The load parameters are listed in Table 3. Under each load condition, the servo system is tested for tracking 1 rad/s, 3.14 rad/s and 6.28 rad/s slope position commands respectively. The PI controller, utilized in the position/ velocity loop, is used for performance comparison. Although different controllers are used for the position and velocity loops, the same PI controller is used in the current loop. The parameters of the controllers are tuned by the trial-and-error method to restrain load torque disturbances and improve steady-state precision. For a fair comparison, the performance of the two controllers is similar when tracking 1 rad/s slope command under load 1. Then all the control parameters are fixed for the

**TABLE 4.** Parameters of the controllers.

| | |
|---|---|
| Current PI Controller | |
| Current loop $k_{pc}$ | 1.5 |
| Current loop $k_{ic}$ | 0.07 |
| Position/ Velocity PI Controller | |
| Velocity loop $k_{pv}$ | 10.0 |
| Velocity loop $k_{iv}$ | 0.15 |
| Position loop $k_{pp}$ | 0.2 |
| Position loop $k_{ip}$ | 0.002 |
| NTSMC+PAC | |
| $r$ | 0.08 |
| $\varepsilon$ | 0.1 |
| $p$ | 5 |
| $q$ | 3 |
| $k_1$ | 10 |
| $k_2$ | 0.02 |
| $r_{adp}$ | 0.2 |

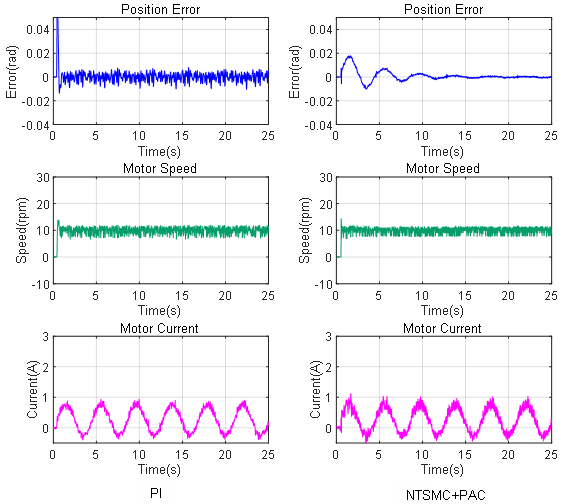


**FIGURE 9.** Experimental results of 1 rad/s slope input under Load 1.

position-tracking test under different loads. The parameters used in the experiments are listed in Table 4.

$\theta_d$ = 1 rad/s, 3.14 rad/s and 6.28 rad/s slope signals are selected as the desired position commands. The comparative results under periodic load 1 are shown in Figure 9 ∼ Figure 11. To obtain better control performance during load variations, the gain parameters of the PI controller are set high. From Figure 9, it can be observed that in the steady state, the tracking error of NTSMC+PAC is much smaller than the PI controller. As shown in Figure 10 ∼ Figure 11, despite the high gain parameters of the PI controller being set, the tracking errors show periodic peaks as the instruction increases, and the higher the instruction is, the larger the peak error becomes. As a result of the periodic adaptive compensation, the tracking precision of NTSMC is much

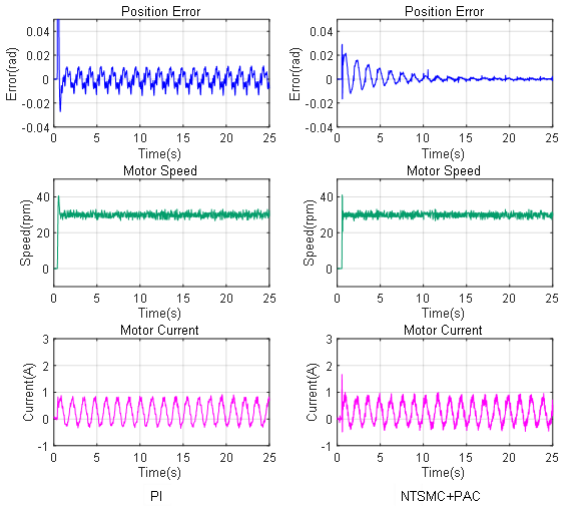


**FIGURE 10.** Experimental results of 3.14 rad/s slope input under Load 1.

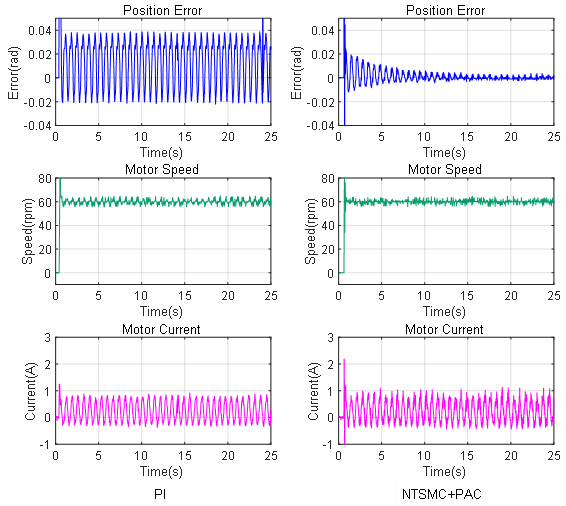


**FIGURE 11.** Experimental results of 6.28 rad/s slope input under Load 1.

**TABLE 5.** Tracking performance of PI and NTSMC+PAC.

| Position Command | Load | Mean Error($10^{-3}$ rad) | | RMS Error($10^{-3}$ rad) | |
|---|---|---|---|---|---|
| | | PI | NTSMC +PAC | PI | NTSMC +PAC |
| 1 rad/s | Load1 | 0.32 | 0.1 | 5.8 | 4.3 |
| 3.14 rad/s | Load1 | 0.87 | 0.76 | 14 | 4.7 |
| 6.28 rad/s | Load1 | 13.9 | 1.1 | 32.7 | 5.9 |
| 1 rad/s | Load2 | 0.34 | 0.23 | 6.5 | 6.3 |
| 3.14 rad/s | Load2 | 1 | 0.8 | 17.6 | 7.1 |
| 6.28 rad/s | Load2 | 29.1 | 1.1 | 57.1 | 9.0 |

better than that of the PI controller, and the tracking error decreases gradually as the motor spins. Compared with the PI controller, better tracking performance of the control method is obtained during the position command variations.

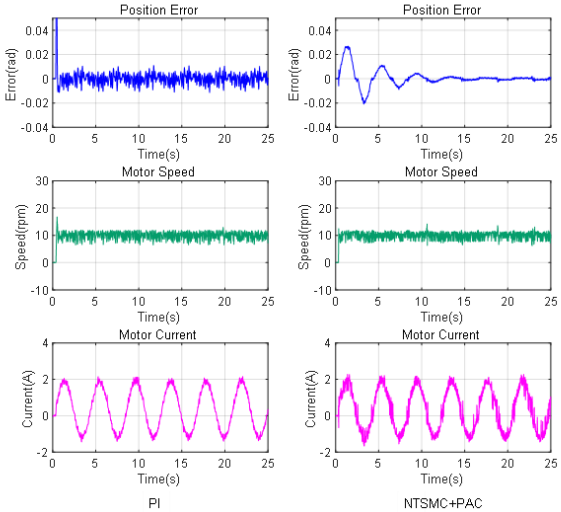


**FIGURE 12.** Experimental results of 1 rad/s slope input under Load 2.

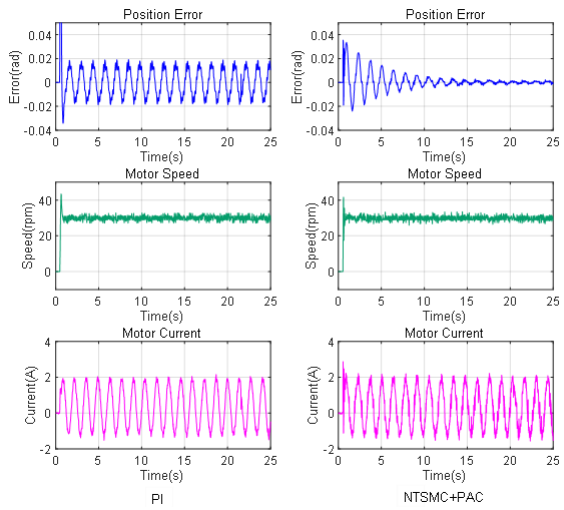


**FIGURE 13.** Experimental results of 3.14 rad/s slope input under Load 2.

Under periodic load 2 conditions, experiments are also carried out. The response curves are shown in Figure 12 ∼ Figure 14. From the figures, it can be observed that, as the periodic load torque increases, the peak error of the PI controller increases greatly compared with the situation under periodic load 1. When the NTSMC+PAC is applied, however, there is little change. As the motor spins, the tracking errors can still be reduced into the small error band gradually. Better tracking performance of the proposed method is also shown in the experiments.

To quantitatively analyze the results, two indexes, including the mean error (i.e. ME= $\frac{1}{n}\sum_{i=1}^{n} e(i)$) and the root mean squared error (i.e., RMSE= $\sqrt{\frac{1}{n}\sum_{i=1}^{n} e(i)^2}$ ), are introduced. The symbol n denotes the total amount of the data. The performance indexes of all experimental results are listed in Table 5. The NTSMC+PAC generates smaller ME and RMSE under different commands and load conditions. In addition, all the

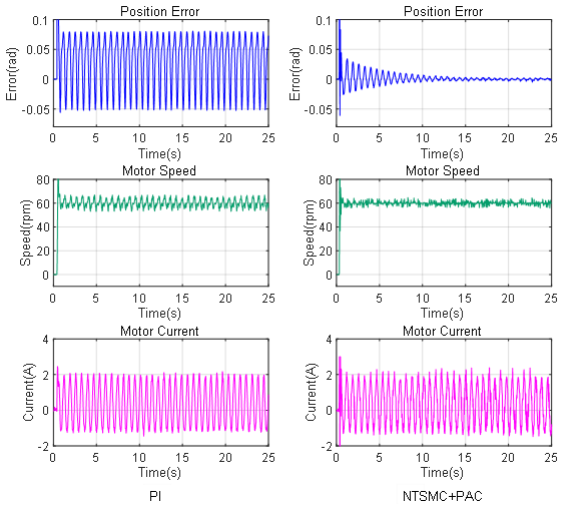


**FIGURE 14.** Experimental results of 6.28 rad/s slope input under Load 2.

error indexes become larger with the increase of command and load conditions. However, the index growth rate of the NTSMC+PAC is less than that of the PI controller. The better ability to adapt to command and load variations of the NTSMC+PAC is demonstrated by the experimental results.

## VI. CONCLUSION

In this paper, a novel position tracking control strategy based on NTSMC with PAC is present. Initially, the mathematical model of the servo system under periodic loads is analyzed. Subsequently, the NTSMC+PAC based on this model is proposed. A new reaching law based on error bands is also developed. The stability of the servo system under the proposed control scheme is verified. The effectiveness of the method is confirmed by simulations first, followed by experimental results. This work offers a solution to enhance tracking performance of servo systems under periodic disturbing torque. Nonetheless, given the executability of control algorithms on microcontroller platforms, the controller design process exhibits a certain level of conservatism. Future research will aim to diminish this conservatism in controllers while augmenting the feasibility of algorithms on microcontroller platforms. Moreover, we aim to extend the proposed scheme to a broader range of servo systems, including high-precision rotating platforms, stable platforms, industrial robots, and so on.

## REFERENCES

[1] C. Dai, T. Guo, J. Yang, and S. Li, "A disturbance observer-based current-constrained controller for speed regulation of PMSM systems subject to unmatched disturbances," *IEEE Trans. Ind. Electron.*, vol. 68, no. 1, pp. 767–775, Jan. 2021.

[2] J. Hang, J. Zhang, M. Xia, S. Ding, and W. Hua, "Interturn fault diagnosis for model-predictive-controlled-PMSM based on cost function and wavelet transform," *IEEE Trans. Power Electron.*, vol. 35, no. 6, pp. 6405–6418, Jun. 2020.

[3] Y. Zhang, Z. Yin, C. Bai, G. Wang, and J. Liu, "A rotor position and speed estimation method using an improved linear extended state observer for IPMSM sensorless drives," *IEEE Trans. Power Electron.*, vol. 36, no. 12, pp. 14062–14073, Dec. 2021.

[4] Y. Yan, J. Yang, Z. Sun, C. Zhang, S. Li, and H. Yu, "Robust speed regulation for PMSM servo system with multiple sources of disturbances via an augmented disturbance observer," *IEEE/ASME Trans. Mechatronics*, vol. 23, no. 2, pp. 769–780, Apr. 2018.

[5] M. Liu, K. W. Chan, J. Hu, W. Xu, and J. Rodriguez, "Model predictive direct speed control with torque oscillation reduction for PMSM drives," *IEEE Trans. Ind. Informat.*, vol. 15, no. 9, pp. 4944–4956, Sep. 2019.

[6] S. Wang, H. Yu, J. Yu, J. Na, and X. Ren, "Neural-network-based adaptive funnel control for servo mechanisms with unknown dead-zone," *IEEE Trans. Cybern.*, vol. 50, no. 4, pp. 1383–1394, Apr. 2020.

[7] S. Wang, L. Tao, Q. Chen, J. Na, and X. Ren, "USDE-based sliding mode control for servo mechanisms with unknown system dynamics," *IEEE/ASME Trans. Mechatronics*, vol. 25, no. 2, pp. 1056–1066, Apr. 2020.

[8] R.-E. Precup, R.-C. David, R.-C. Roman, A.-I. Szedlak-Stinean, and E. M. Petriu, "Optimal tuning of interval type-2 fuzzy controllers for nonlinear servo systems using slime mould algorithm," *Int. J. Syst. Sci.*, vol. 54, no. 15, pp. 2941–2956, Jun. 2021.

[9] S. Wang and J. Na, "Parameter estimation and adaptive control for servo mechanisms with friction compensation," *IEEE Trans. Ind. Informat.*, vol. 16, no. 11, pp. 6816–6825, Nov. 2020.

[10] W. Sun, Y. Liu, and H. Gao, "Constrained sampled-data ARC for a class of cascaded nonlinear systems with applications to motor-servo systems," *IEEE Trans. Ind. Informat.*, vol. 15, no. 2, pp. 766–776, Feb. 2019.

[11] I. A. Zamfirache, R.-E. Precup, R.-C. Roman, and E. M. Petriu, "Reinforcement learning-based control using Q-learning and gravitational search algorithm with experimental validation on a nonlinear servo system," *Inf. Sci.*, vol. 583, pp. 99–120, Jan. 2022.

[12] D. Wu and K. Chen, "Frequency-domain analysis of nonlinear active disturbance rejection control via the describing function method," *IEEE Trans. Ind. Electron.*, vol. 60, no. 9, pp. 3906–3914, Sep. 2013.

[13] A. Apte, V. A. Joshi, H. Mehta, and R. Walambe, "Disturbance-observer-based sensorless control of PMSM using integral state feedback controller," *IEEE Trans. Power Electron.*, vol. 35, no. 6, pp. 6082–6090, Jun. 2020.

[14] Y. Wang, L. Zheng, H. Zhang, and W. X. Zheng, "Fuzzy observer-based repetitive tracking control for nonlinear systems," *IEEE Trans. Fuzzy Syst.*, vol. 28, no. 10, pp. 2401–2415, Oct. 2020.

[15] X. Zhang, L. Sun, K. Zhao, and L. Sun, "Nonlinear speed control for PMSM system using sliding-mode control and disturbance compensation techniques," *IEEE Trans. Power Electron.*, vol. 28, no. 3, pp. 1358–1365, Mar. 2013.

[16] V. Q. Leu, H. H. Choi, and J.-W. Jung, "Fuzzy sliding mode speed controller for PM synchronous motors with a load torque observer," *IEEE Trans. Power Electron.*, vol. 27, no. 3, pp. 1530–1539, Mar. 2012.

[17] W. Xu, Y. Jiang, and C. Mu, "Novel composite sliding mode control for PMSM drive system based on disturbance observer," *IEEE Trans. Appl. Supercond.*, vol. 26, no. 7, pp. 1–5, Oct. 2016.

[18] B. Zhang, Y. Pi, and Y. Luo, "Fractional order sliding-mode control based on parameters auto-tuning for velocity control of permanent magnet synchronous motor," *ISA Trans.*, vol. 51, no. 5, pp. 649–656, Sep. 2012.

[19] Y. Jiang, W. Xu, C. Mu, and Y. Liu, "Improved deadbeat predictive current control combined sliding mode strategy for PMSM drive system," *IEEE Trans. Veh. Technol.*, vol. 67, no. 1, pp. 251–263, Jan. 2018.

[20] G. Wang, Z. Zuo, and C. Wang, "Robust consensus control of second-order uncertain multiagent systems with velocity and input constraints," *Automatica*, vol. 157, Nov. 2023, Art. no. 111226.

[21] G. Wang, "Distributed control of higher-order nonlinear multi-agent systems with unknown non-identical control directions under general directed graphs," *Automatica*, vol. 110, Dec. 2019, Art. no. 108559.

[22] Q. Shen, P. Shi, and C. Peng Lim, "Fuzzy adaptive fault-tolerant stability control against novel actuator faults and its application to mechanical systems," *IEEE Trans. Fuzzy Syst.*, vol. 32, no. 4, pp. 2331–2340, Apr. 2024.

[23] J. Zhu, Q. Shen, T. Zhang, and Y. Yi, "Decentralized finite-time adaptive neural FTC with unknown powers and input constraints," *Inf. Sci.*, vol. 656, Jan. 2024, Art. no. 119909.

[24] T. Satheesh, R. Sakthivel, S. Harshavarthini, R. Manikandan, and D. J. Almakhles, "Antiwindup compensator-based control for periodic piecewise delayed systems with input saturations," *J. Dyn. Syst., Meas., Control*, vol. 145, no. 2, Feb. 2023, Art. no. 021003.

[25] T. Satheesh, R. Sakthivel, N. Aravinth, and M. Chadli, "Design of proportional integral observer-based resilient control for periodic piecewise time-varying systems: The finite-time case," *Int. J. Robust Nonlinear Control*, vol. 34, no. 2, pp. 1169–1195, Oct. 2023.
[26] T. Satheesh, R. Sakthivel, N. Aravinth, and H. R. Karimi, "Unified synchronization and fault-tolerant anti-disturbance control for synchronization of multiple memristor-based neural networks," *Int. J. Robust Nonlinear Control*, vol. 34, no. 4, pp. 2849–2864, Nov. 2023.
[27] H. Liu and S. Li, "Speed control for PMSM servo system using predictive functional control and extended state observer," *IEEE Trans. Ind. Electron.*, vol. 59, no. 2, pp. 1171–1183, Feb. 2012.
[28] Y. Chen, Q. Q. Xie, F. Zhou, and X. Liu, "Research on dead-zone compensation of AC servo system based on voltage feed forward decoupling and FOC," *Przeglad Elektrotechniczny*, vol. 88, no. 7A, pp. 86–89, 2012.
[29] M. Seilmeier and B. Piepenbreier, "Sensorless control of PMSM for the whole speed range using two-degree-of-freedom current control and HF test current injection for low-speed range," *IEEE Trans. Power Electron.*, vol. 30, no. 8, pp. 4394–4403, Aug. 2015.
[30] S. S. Xu, C.-C. Chen, and Z.-L. Wu, "Study of nonsingular fast terminal sliding-mode fault-tolerant control," *IEEE Trans. Ind. Electron.*, vol. 62, no. 6, pp. 3906–3913, Jun. 2015.

**WEI CHEN** was born in Jiangsu, China, in 1986. He received the Ph.D. degree from Nanjing University of Science and Technology (NJUST), Nanjing, China, in 2014.

He is currently a Senior Engineer with the College of Electrical Engineering, NJUIT. His current research interests include motor drive and servo control techniques.

**DEJIN TAO** was born in Jiangsu, China, in 1985. He received the Ph.D. degree from Nanjing University of Science and Technology (NJUST), Nanjing, China, in 2013.

He is currently a Research Professor with The 28th Research Institute of China Electronics Technology Group Corporation, Nanjing. His current research interests include command control and command systems.

**BO TANG** was born in Jiangsu, China, in 1990. He received the Ph.D. degree from Nanjing University of Science and Technology (NJUST), Nanjing, China, in 2019.

He is currently a Lecturer with the College of Electrical Engineering, NJUIT. His current research interest includes railgun launch technology.